Determination of Isothermal Sections of Nickel Rich Portion of Ni-Cr-Mo System by Analytical Electron Microscopy

M. RAGHAVAN, R. R. MUELLER, G. A. VAUGHN, and S. FLOREEN

Ternary sections at 1523 K (1250 °C) and 1123 K (850 °C) of the nickel rich portion of the Ni-Cr-Mo system were determined by analytical electron microscopy (AEM) consisting of X-ray microanalysis and Convergent Beam Diffraction (CBD). At 1523 K, both the gamma solvus boundary and the type of intermetallic (delta, P, and sigma) phases present were in good agreement with some of the previous investigations. However, the three-phase fields were clearly defined only by AEM. At 1123 K, the gamma phase exhibited decreased solubility of Cr and Mo, as expected, but interestingly, the formation of a fourth intermetallic, mu phase, was observed along with the delta, P, and sigma phases. The CBD analyses of these phases and comparison of the results of the present investigation with the published experimental and theoretical diagrams are presented.

I. INTRODUCTION

THE determination of phase diagrams to understand the phase equilibria in metallic system has been of paramount interest in many areas of metallurgical research. Phase diagrams in binary, ternary, and multicomponent systems have been determined using one or a combination of the conventional techniques such as dilatometry, optical metallography, thermal analysis, high and low temperature X-ray diffraction, and magnetic measurements.[1-4] The theories behind these techniques are different, but they essentially consist of defining the phase boundaries by detecting changes in the structure and/or properties of a bulk sample brought about by phase transformation(s). Although these techniques have been extensively used to define the phase diagrams in the past, they suffer from some basic disadvantages. A few of the general limitations of these techniques are listed below:

(1) Inability to uniquely determine the composition and crystal structure of individual phases, especially in multicomponent systems.
(2) Measurement of phase boundaries in the bulk samples assumes uniform composition throughout the sample. Macrosegregation in the samples could affect the results.
(3) Since the accuracy of defining the phase boundaries depends upon the number of samples selected, a relatively larger number of samples are required.
(4) There are difficulties in the accurate determination of the compositions of triple points and three- and four-phase regions in ternary and quarternary systems.
(5) Attainment of equilibrium is difficult to establish.

It will be attractive to develop methods in which all or most of these limitations can be overcome. Modern probe forming analytical electron microscopes are capable of accurately determining the composition and crystal structure of individual phases with excellent spatial resolution. These capabilities of the electron microscope can be effectively used to determine the boundaries separating the different phase regions in alloy systems avoiding most of the disadvantages of the conventional techniques listed above. However, the major concerns in using analytical electron microscopes for quantitative chemical analysis have been (i) the contribution of the spurious X-rays to the measured spectra and (ii) the accuracy of the subsequent quantitation. These concerns have been the subject of many previous investigations and the results were recently discussed.[5-8] It was pointed out that the spurious X-rays in an analytical electron microscope can be minimized by careful microscope design and selection of experimental conditions. The three major sources of the spurious X-rays which have to be contended with are (a) uncollimated electrons, (b) uncollimated hard X-rays, and (c) continuum X-rays. The uncollimated electrons and hard X-rays are generally controlled by using spray and thick C2 apertures, and the contribution from these sources can be estimated by measuring the hole-count.

The effect of continuum X-ray production on the spurious X-rays can be minimized by using a low background beryllium holder and by using zero tilt on the sample. In order to implement the latter recommendation, it is necessary to have an X-ray detector which is moved out of the detector plane. The X-ray detector used in the present investigation has a take-off angle of 20 degrees to the horizontal axis. The effect of the X-ray continuum on the generation of spurious X-rays can be determined by comparing the analysis from precipitates in a thin sample to the analysis of the extracted residue of the same precipitates supported by a carbon film on a beryllium grid. As will be described later, the spurious X-rays from these sources were not found to be significant.

The approach used in the study is described in Figure 1, which shows a schematic section of the Ni-Cr-Mo system based on previously published studies.[9,10] The procedure consists of selecting alloy compositions in the two- and three-phase gamma + intermetallic phase regions, exposing them to the desired temperature for an extended period of time to attain equilibrium, and then determining the chemical composition and crystal structure of the phases present by X-ray microanalysis and convergent beam diffraction (CBD), respectively. For illustration, an alloy composition (point A) contains two phases — the austenite

M. RAGHAVAN and R. R. MUELLER are with Exxon Research and Engineering Company, LG 362, Route 22 East, Annandale, NJ 08801. G. A. VAUGHN is with Exxon Production Research Company, P. O. Box 2189, Houston, TX 77001. S. FLOREEN is with International Nickel Company, Sterling Forest, Suffern, NY 10901.

Manuscript submitted July 28, 1983.

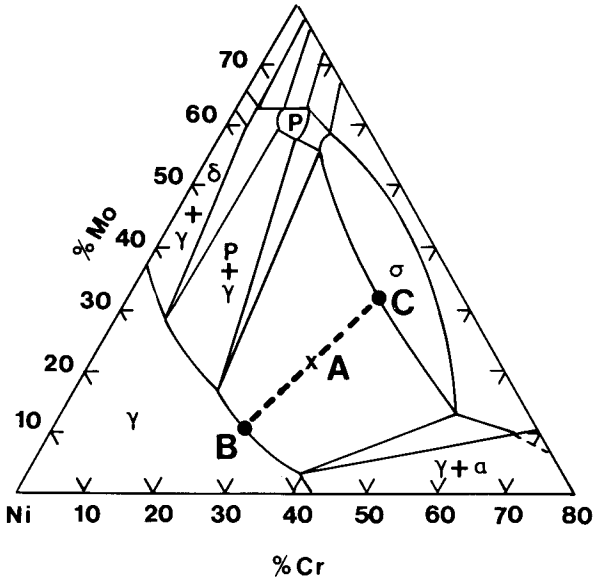

Fig. 1 — Schematic isothermal section of the Ni-Cr-Mo ternary system.[9,10]

matrix and an intermetallic phase. As shown in the figure, the composition of the austenite (point B) and the composition of the intermetallic phase (point C) define their respective boundaries. By selecting several compositions in the two (and three-)-phase fields, the phase boundaries can be mapped. The technique has a special advantage in determining the three-phase regions. From one alloy composition in this region, it is possible to determine the entire three-phase field by measuring the compositions of all the three phases in equilibrium, because the composition of the three phases in equilibrium in a ternary system are invariant at any given temperature. The unique identification of intermetallic phases can be done by determining their crystal structure. This present article describes a detailed analytical electron microscopy study conducted to determine the isothermal sections of the nickel-rich portion of the Ni-Cr-Mo phase diagram at 1523 K (1250 °C) and 1123 K (850 °C).

II. EXPERIMENTAL PROCEDURE

Ternary alloys for the investigations were prepared from pure element powders by vacuum arc melting 50 gm buttons. Seven alloy compositions were selected along each of the two tie-lines — Series A in which Cr + Mo = 40 pct and Series B in which Cr + Mo = 50 pct.* The nominal compositions of the alloys are listed in Table I. The original intention of the alloy selection was to use Series A for the 1123 K section and Series B for the 1523 K section so as to form a reasonable volume fraction of the intermetallic phases (20 to 40 pct) at these temperatures. However, both the alloy series were eventually used to determine the phase boundaries. Slices, approximately 4 mm thick, were cut from the buttons and heat treated in an argon atmosphere. All the samples were annealed at 1523 K for 100 hours to homogenize the samples. Portions of these homogenized samples were retained to determine the 1523 K section while the remainder were exposed to 1123 K for 1000 hours. Samples of the heat treated slices were mounted for optical metallography and electron microprobe analysis. Samples for X-ray microanalysis were prepared by mechanically grinding the slices to about ~150 μm, electropolishing, and subsequent ion milling. Ion milling was necessary to uniformly thin the second phase particles suitable for X-ray microanalysis and electron diffraction.

*Unless specified otherwise, compositions refer to wt pct.

Table I. Nominal Alloys Composition

Sample Numbers	Composition, Wt Pct		
	Ni	Cr	Mo
1A	60	5	35
2A	60	10	30
3A	60	15	25
4A	60	20	20
5A	60	25	15
6A	60	30	10
7A	60	35	5
1B	50	5	45
2B	50	10	40
3B	50	15	35
4B	50	20	30
5B	50	25	25
6B	50	30	20
7B	50	35	15

The samples were analyzed in an EM400T electron microscope fitted with a field emission gun and equipped with a 20 degrees take-off angle EDAX X-ray detector and a 9100 analyzer. All the analyses were conducted in a low background holder at a tilt angle of zero degree. X-ray spectra were generated with an approximately 12.5 nm electron probe in the TEM mode using a "thick" 70 μm C2 aperture. The spectra were collected until the tallest channel reached 2500 counts and the typical acquisition time was about 100 seconds, live time.

Peak intensities were measured by manually setting windows for the K_α peaks of Cr, Ni, and Mo and subtracting the background. The intensities were corrected for absorption and absolute concentrations calculated based on k values[11] measured using single phase Ni-Cr-Mo alloy standards. The chemical compositions of the standards were independently determined both by electron microprobe and wet chemical analyses. Convergent beam diffraction analysis was carried out using procedures described recently.[12,13,14]

III. RESULTS

A. *Scanning Microscopy*

Polished samples of the heat treated slices were examined in a scanning electron microscope to determine the distribution of the second-phase particles. Figure 2 shows a typical microstructure of alloy #5B annealed at 1523 K. The intermetallic phases were present as large 25 μm spherical particles, and their size and distribution were uniform throughout the sample. Qualitative X-ray analysis also showed that the composition of the intermetallic particles was also uniform throughout the sample, and, within experimental error, no significant chemical or microstructural inhomogeneities were observed in the samples.

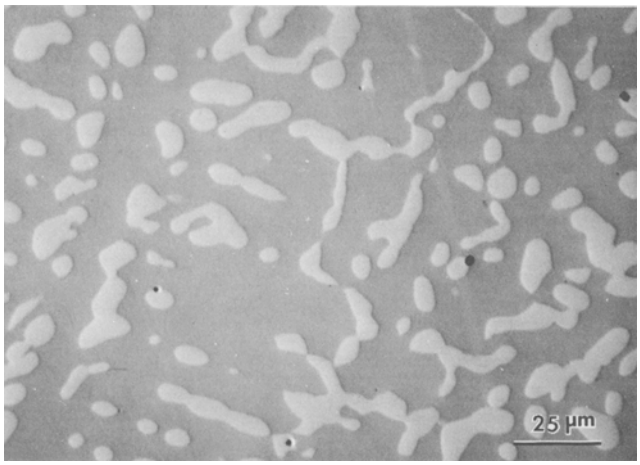

Fig. 2—Back-scattered electron image of coarse precipitates in alloy #5B aged at 1523 K (1250 °C) for 100 h.

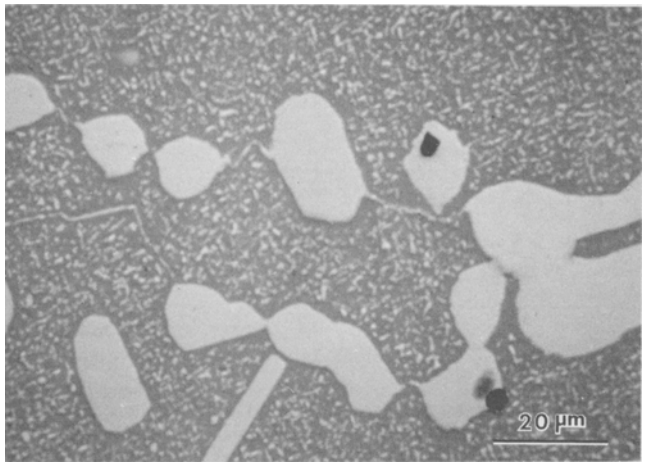

Fig. 3—Back-scattered electron image of coarse and fine precipitates in alloy #5B annealed at 1523 K (1250 °C) for 100 h, and aged at 1123 K (850 °C) for 1000 h.

Samples heat treated at 1123 K showed two particle distributions (Figure 3). The large spherical particles which were present after the 1523 K anneal were retained and, in addition, a finer dispersion of particles had precipitated at 1123 K. The size of these finer precipitates ranged from 0.5 to 2 μm. Due to their small size, it was not possible to compare the composition of the fine precipitates with that of coarse ones in the scanning microscope. As will be described later, transmission electron microscopy analysis showed that the composition and nature of the coarse and fine precipitates were identical.

B. *Scanning Transmission Electron Microscopy*

Preliminary analysis was carried out to clarify two common concerns experienced in quantitative X-ray microanalysis. The first is the contribution of the spurious X-rays generated from the sample away from the region analyzed, particularly in the thin samples. Secondly, it is necessary to demonstrate that the precipitates and matrix have attained equilibrium at the desired temperature and their average concentrations do represent their equilibrium compositions. The initial experiments were directed to answer these questions. As mentioned previously, the contribution of the spurious X-rays from uncollimated electrons and X-rays can be determined by analyzing the hole count. Following the procedure described by Zaluzec,[7] the fractions of the hole-counts for the Cr, Ni, and Mo K_α peaks to the corresponding peaks generated in a thin sample were determined to be less than 1.2 pct, and this value was suggested to be an acceptable level of background X-rays. Therefore, it was concluded that the uncollimated electrons and X-rays were not contributing to significant levels of spurious signal. The second source of spurious X-rays arises from the interaction of the entire sample with the continuum X-rays, and to determine its contribution, X-ray microanalysis was conducted on precipitates both in thin samples and also on the residues extracted from the bulk samples. Four alloys aged at 1523 K for 100 hours + 1123 K for 1000 hours were selected for this comparison, and the results are tabulated in Table II. It should be mentioned that the extracted particles were generally too thick for electron transparency, and only the edges were thin enough for the analysis. In obtaining X-ray spectra from the extracted precipitates, care was taken to ensure that the X-ray detector had a clear line of sight to the region analyzed. Comparison of the precipitates analyzed in the thin foil and extracted residue indicates that the precipitate compositions were remarkably comparable, within the experimental scatter. Based on this comparison, it was concluded that the use of thin samples does not cause any significant levels of spurious X-rays and provides reasonably accurate X-ray microanalysis. The rest of the analysis in the present study was conducted using thin film samples.

Since phase diagrams depict equilibrium conditions among phases, the initial studies in the investigation were directed at determining if the phases had reached equilibrium after the heat treatments. To evaluate this, concentration profiles of Cr and Mo were generated across a precipitate-matrix interface using a probe size in the STEM estimated to be 1.0 to 1.5 nm in sample #2A that was aged at 1523 K for 100 hours and subsequently at 1123 K for 1000 hours. A typical concentration profile is shown in Figure 4. The horizontal error bars represent the beam broadening calculated based on the single scattering model

Table II. Comparison of X-Ray Microanalysis in Thin Samples and Extracted Residue Composition, Wt Pct ($\pm\sigma$)

Sample Designation	Extract			Thin Foil		
	Ni	Cr	Mo	Ni	Cr	Mo
1B	38.4 (0.6)	4.4 (0.3)	57.2 (0.5)	38.6 (0.7)	4.6 (0.5)	56.8 (0.7)
4B	32.8 (0.4)	18.2 (0.7)	49.0 (0.4)	32.3 (1.0)	17.0 (0.7)	50.7 (0.9)
6B	32.2 (0.3)	36.5 (0.3)	31.3 (0.2)	32.9 (0.9)	34.5 (0.8)	32.6 (1.0)
7B	30.9 (0.7)	43.4 (0.5)	25.7 (0.3)	31.6 (1.1)	42.8 (1.2)	25.6 (0.8)

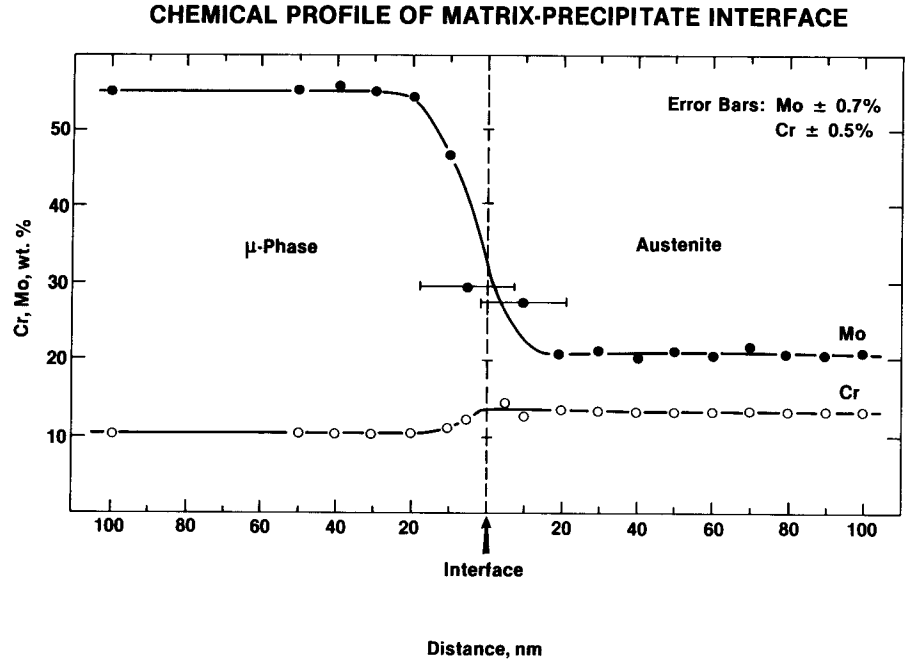

Fig. 4—Compositional profile of μ-phase/austenite interface in sample #2A determined with 0.5 nm STEM probe. Error bars: Mo ± 0.7 pct, Cr ± 0.5 pct.

of Goldstein *et al.*[15] and the profiles showed a smooth transition from the matrix to the precipitate. Cr and Mo profiles were also generated across several austenite-austenite grain boundaries and the results confirmed that there was no depletion or enrichment of these elements at the boundaries. These results indicated that the phases had reached equilibrium at 1123 K and 1523 K.

C. *1523 K (1250 °C) Section*

The bright-field microstructure of the alloy samples (except for samples #6A and #7A which were single phase austenite) showed coarse intermetallic phases (~25 μm) separated by comparable regions of austenite. X-ray spectra were obtained from the austenite and intermetallic phases, and Table III lists the compositions of the austenite phase and also the type and compositions of the intermetallic phases present in the alloy samples. These data were used to plot the 1523 K section as shown in Figure 5. Alloys which were in the single phase austenite region (#6A and #7A) are not included in the plot. The austenite compositions defined the gamma solvus boundary with very little scatter while defining the boundaries of the intermetallic phases was found to be slightly more difficult due to a higher degree of scatter in the data.

The intermetallic phase in the alloy containing the lowest nominal Cr content was found to be the delta phase. Shoemaker and Shoemaker[16] determined the crystal structure of δ phase to be orthorhombic with $a = b = 0.908$ nm, $c = 0.8852$ nm, belonging to the space group $P_{2_12_12_1}$. The delta phase contained very few faults compared to the other intermetallic phases. Figure 6 shows the [010] CBD pattern of the δ phase. The pattern obtained with a 20 μm C2 aperture, Figure 6(a), shows a square network of spots in the zero layer Laue Zone (ZOLZ). A closer examination also shows that the spots in the first order Laue Zone (FOLZ) also consisted of a square array of spots and

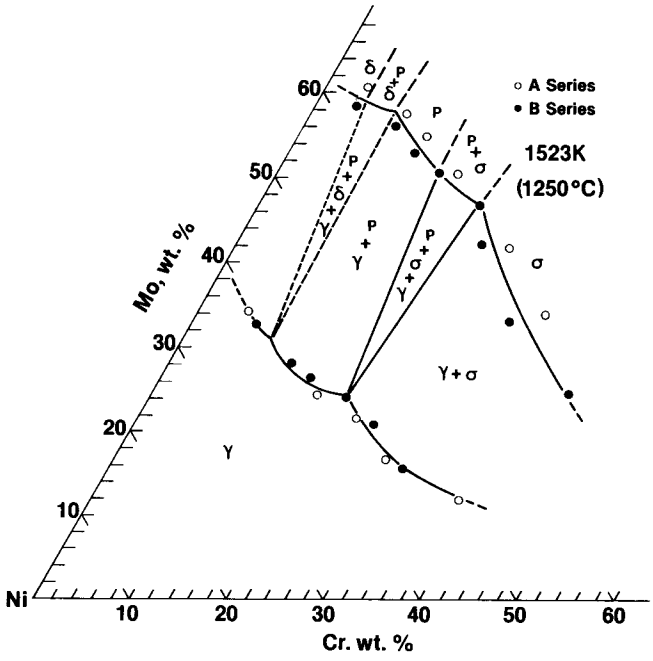

Fig. 5—1523 K (1250 °C) section of the Ni-Cr-Mo ternary system determined in the present investigation.

that they superposed exactly on the spots in the ZOLZ. This can be established by locating the FOLZ reflections along the edges and diagonals of the ZOLZ (square) pattern as discussed previously.[12,17] The CBD pattern shown in Figure 6(b) was taken under exactly the same conditions as shown in Figure 6(a) except with a 150 μm C2 aperture. The pattern clearly shows a two-fold symmetry with two mirrors marked M_1 and M_2. The H^{-1} value* was calculated as 0.9 nm which, in the present case, corresponds to

*H refers to the reciprocal lattice layer spacing parallel to the electron beam. H^{-1} (Å) is the real space correspondence.[12,13]

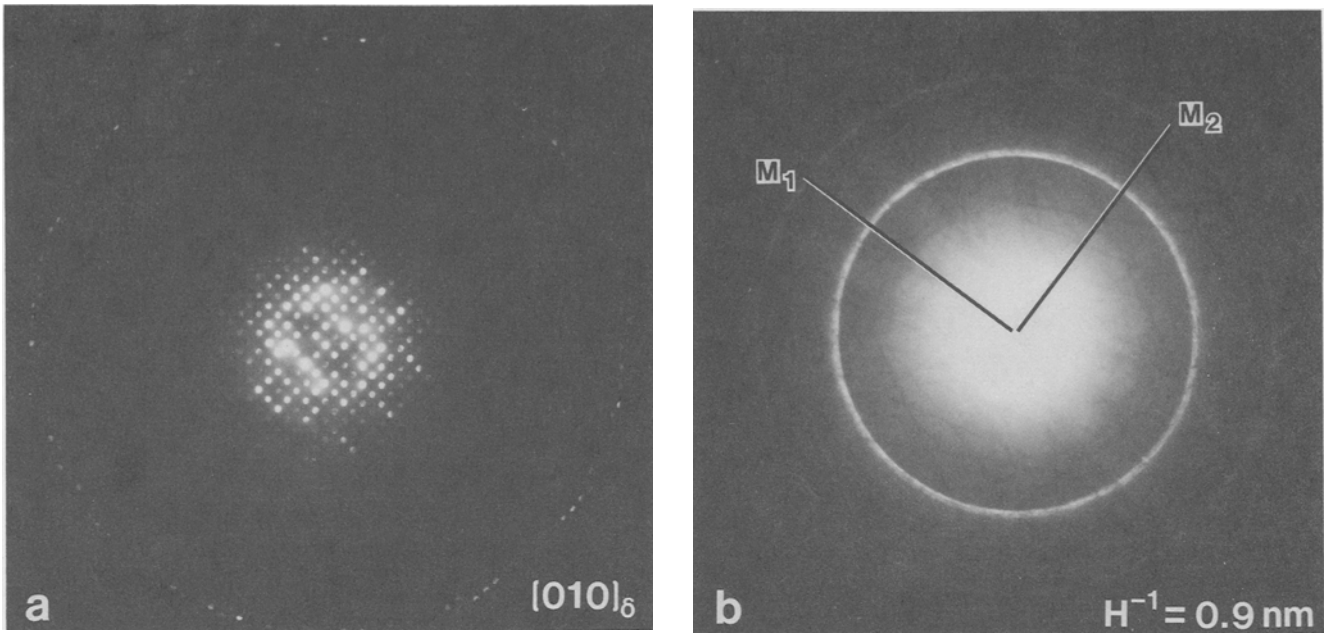

Fig. 6—Convergent beam diffraction (CBD) pattern from $[010]_\delta$ using (*a*) 20 μm and (*b*) 150 μm condenser apertures. The mirror planes M_1 and M_2 indicate that the symmetry is two-fold.

d_{010} = 0.91 nm of the δ phase. It is interesting to note that the zero layer pattern in Figure 6(a) is indexed to consist of (100) and (001) reflections though both these reflections are forbidden by the structure factor. These reflections form by double diffraction in the ZOLZ, and this point will be discussed later. X-ray microanalysis results show that the delta phase contained about 6 pct Cr indicating limited solubility of Cr in this phase.

The next intermetallic phase which formed with increasing Cr concentration of the alloy was determined to be the P phase. The P phase which contained only a few faults was determined by Shoemaker *et al.* to have an orthorhombic crystal structure with a = 0.907 nm, b = 1.698 nm, and c = 0.475 nm belonging to the space group Pbnm.[18] None of the alloys examined contained both the delta and the P phase and, therefore, it was not possible to determine uniquely the three-phase ($\gamma + \delta$ + P) field, and the location of this region was only estimated. The composition range of P was determined to be Cr: 9.1 to 18.4 pct, Ni: 31.2 to 34.5 pct, and Mo: 50.4 to 58.2 pct, and the average chemical formulation can be written down as $Cr\ Ni_2\ Mo_2$ which is in very good agreement with the $Cr_{18}\ Ni_{40}\ Mo_{42}$ reported by Shoemaker.[18] A [010] CBD pattern from the P phase is shown in Figure 7. The inset in the figure shows the ZOLZ obtained using a 20 μm C2 aperture. Again, as observed in the delta phase, the (100) and (001) reflections which are forbidden by the structure factor appear in the ZOLZ by double diffraction. The H^{-1} value was calculated as 0.47 nm in agreement with d_{010} = 0.475 nm. The whole pattern symmetry of the pattern is two-fold.

The third intermetallic compound observed with increasing Cr was the well-known sigma phase which has a tetragonal crystal structure, a = 0.88 nm, c = 0.454 nm and the space group is P4/mnm.[19] The sigma phase contained a relatively higher fault density compared to both the delta and P phases. Alloy #4B was found to contain

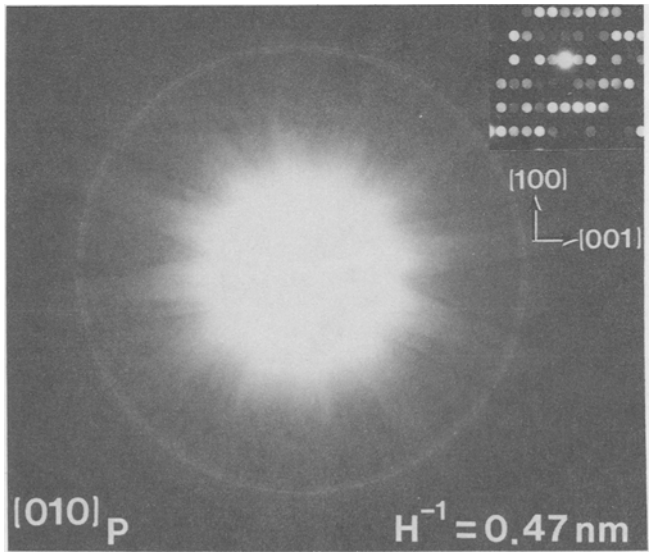

Fig. 7—Convergent beam diffraction (CBD) pattern from $[010]_P$ with ZOLZ (inset).

both the P and sigma phases, and it was therefore possible to determine uniquely the three-phase (γ + P + σ) region as shown in Figure 5. Figure 8 is a bright-field image of these phases coexisting in Alloy #4B. The [001] CBD pattern from the sigma phase is shown in Figure 9. In this pattern, the ZOLZ consists of a square network of (100) and (010) reflections, both of which are forbidden by structure factor. The FOLZ also consists of a square pattern, and careful analysis revealed that, as in the case of the δ phase, the spots in the first layer do superimpose on the zero layer. The H^{-1} value was calculated to be 0.47 nm which is in good agreement with the d_{001} of 0.475 nm, and the whole pattern symmetry was four-fold. The sigma phase had the

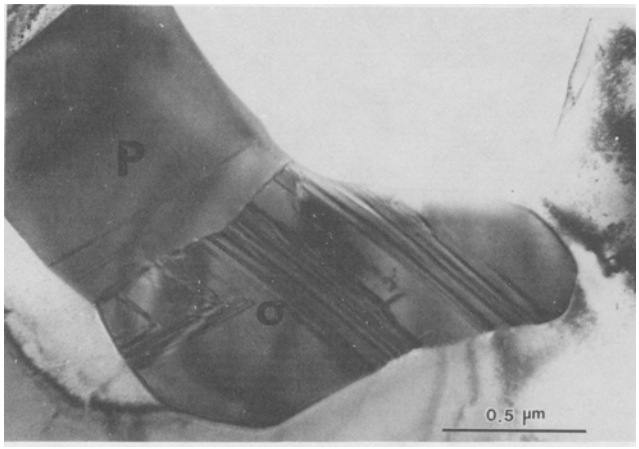

Fig. 8—Bright-field image of specimen #4B aged at 1523 K (1250 °C)/100 h showing P and sigma phases.

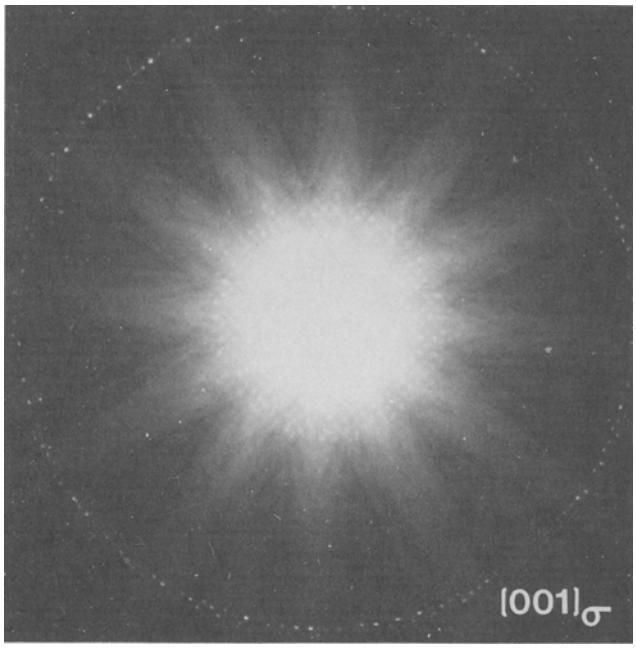

Fig. 9—Convergent beam diffraction (CBD) pattern from $[001]_\sigma$.

widest range of composition compared to the delta and P phases. Such extensive solubility of alloying elements in the sigma phase has been observed previously in several ternary alloy systems.[20]

D. *1123 K (850 °C) Section*

As mentioned previously, samples aged at 1123 K contained two precipitate sizes. The coarse, approximately 25 μm in size, particles had formed at the 1523 K anneal, and the relatively finer distribution of particles had formed after the subsequent 1123 K anneal. Figure 10 is a typical bright-field image of the finer particles in alloy #3A which ranged in size from about 0.5 to 2.0 μm. Preliminary studies showed that the compositions of the coarse and fine particles were similar within the experimental scatter of the analysis and, therefore, the average compositions of these precipitates are presented here. Table IV lists the compositions of the austenite and the type and composition of the intermetallic phases in each alloy. The data are plotted in the ternary section shown in Figure 11.

Fig. 10—Bright-field image of fine μ-phase precipitates in alloy #3A aged at 1523 K (1250 °C)/100 h + 1123 K (850 °C)/1000 h.

As in the case of the 1523 K section, the intermetallic phase(s) found in the lowest Cr containing alloys was the delta phase, and the compositions of the delta phase at 1123 and 1523 K were very comparable. The main difference in the 1123 K section compared to the 1523 K section was that the second intermetallic phase which formed with the increasing Cr content of the alloy was found to be a μ phase instead of the P phase. The μ phase was extensively faulted and has a rhombohedral crystal structure (a = 0.475 nm and c = 2.457 nm). The formation of the μ phase has been reported in Fe-W, Fe-Mo, and Co-Mo Co-W binary systems with a A_7B_6 stoichiometry.[20] The fault density of the μ phase was the highest among all the intermetallic phase and is a characteristic morphological feature to distinguish this phase. Figure 12 is a CBD pattern of the μ phase and the inset is the ZOLZ. The H^{-1} value for the FOLZ was calculated to be 2.54 nm which in this orientation corresponds to the spacing of the c axis of the crystal. The ZOLZ spot pattern shows a hexagonal network of spots which erroneously suggests a six-fold symmetry. A closer examination of the whole pattern of the CBD indicates that the axis is only a three-fold axis, consistent with the symmetry for a rhombohedral crystal. From the diffraction information available in Figure 12 such as the whole pattern symmetry, the H^{-1} value, and the d-spacings of the reflections in the ZOLZ, it is possible not only to deduce the crystal structure but also its lattice spacings. Interestingly, at 1123 K, alloy #1A consisted of both the δ and μ phases, and it was therefore possible to define uniquely the three-phase field ($\gamma + \delta + \mu$) region as shown in Figure 11. The

Table III. Precipitate and Matrix Composition at 1523 K (1250 °C)

Sample Number	Precipitate	Composition, Wt Pct (±σ)					
		Matrix			Precipitate		
		Ni	Cr	Mo	Ni	Cr	Mo
1A	δ	60.3 (0.5)	5.6 (0.4)	34.1 (0.9)	35.3 (0.2)	4.1 (0.2)	60.6 (0.4)
2A	P	60.8 (0.2)	11.5 (0.2)	27.7 (0.2)	32.7 (0.9)	9.1 (0.2)	58.2 (0.9)
3A	P	58.5 (0.4)	17.0 (0.1)	24.5 (0.4)	31.5 (1.2)	13.5 (0.1)	55.0 (1.3)
4A	P	55.5 (0.3)	22.7 (0.4)	21.8 (0.8)	31.2 (0.5)	18.4 (0.5)	50.4 (0.8)
5A	σ	54.6 (1.1)	28.2 (0.2)	17.2 (1.3)	29.4 (0.5)	28.5 (0.5)	42.1 (0.9)
6A	none	60.0 (1.3)	30.2 (0.5)	9.8 (1.1)	—	—	—
7A	none	59.0 (1.2)	35.5 (0.1)	5.5 (0.2)	—	—	—
1B	δ	60.5 (0.4)	6.3 (0.4)	33.2 (0.7)	37.4 (0.6)	4.0 (0.3)	58.6 (0.5)
2B	P	59.4 (0.4)	12.6 (0.4)	28.0 (0.3)	34.6 (0.3)	9.1 (0.1)	53.3 (0.6)
3B	P	58.2 (0.1)	15.6 (0.1)	26.2 (0.4)	34.5 (0.2)	13.0 (0.1)	52.5 (0.1)
4B	P				32.3 (0.2)	17.0 (0.1)	50.7 (0.1)
4B		55.5 (0.5)	20.2 (0.1)	24.3 (0.2)			
4B	σ				30.5 (0.2)	22.5 (0.1)	47.0 (0.3)
5B	σ	54.7 (0.4)	24.6 (0.2)	20.7 (0.2)	32.6 (0.2)	25.4 (0.1)	42.0 (0.3)
6B	σ	54.3 (0.1)	29.8 (0.1)	15.9 (0.1)	33.9 (0.2)	32.5 (0.2)	33.6 (0.2)
7B	σ	49.8 (0.1)	38.0 (0.3)	12.2 (0.2)	31.6 (1.0)	42.8 (0.5)	25.6 (0.8)

Table IV. Precipitate and Matrix Composition at 1123 K (850 °C)

Sample Number	Precipitate	Composition, Wt Pct (±σ)					
		Matrix			Precipitate		
		Ni	Cr	Mo	Ni	Cr	Mo
1A	μ				35.9 (1.3)	5.3 (0.4)	58.8 (1.6)
1A		66.3 (0.4)	5.6 (0.6)	28.1 (1.0)			
1A	δ				36.4 (0.7)	3.6 (0.2)	60.1 (0.6)
2A	μ	65.0 (0.4)	13.8 (0.2)	21.2 (0.4)	35.1 (1.7)	10.5 (0.4)	54.4 (2.0)
3A	μ	62.8 (0.5)	17.3 (0.3)	19.9 (0.8)	32.1 (0.9)	12.4 (0.2)	55.5 (1.0)
4A	μ	61.0 (0.4)	24.8 (0.2)	14.2 (0.5)	31.6 (1.8)	17.1 (0.4)	51.3 (2.2)
5A	μ				30.7 (1.0)	18.9 (1.0)	50.4 (1.0)
5A		60.4 (0.1)	27.8 (0.1)	11.6 (0.1)			
5A	P				30.0 (0.2)	23.9 (0.3)	46.1 (0.3)
6A	σ	56.1 (0.6)	33.3 (0.7)	10.5 (0.5)	28.1 (0.7)	40.0 (0.5)	31.9 (0.2)
7A	none	61.0 (0.7)	33.5 (0.1)	5.5 (0.2)	—	—	—
2B	μ	64.2 (0.4)	14.0 (0.5)	21.8 (0.4)	33.8 (0.8)	10.0 (0.3)	56.2 (0.9)
3B	μ	65.7 (0.3)	16.9 (0.1)	17.4 (0.3)	33.9 (0.1)	12.0 (0.1)	54.5 (0.5)
5B	μ				31.9 (0.3)	18.6 (0.3)	49.5 (0.5)
5B		62.9 (0.1)	25.9 (0.2)	11.2 (0.3)			
5B	P				29.4 (0.6)	25.6 (0.9)	45.0 (0.4)
6B	P				29.1 (0.7)	28.1 (0.4)	42.8 (0.6)
6B		59.2 (0.5)	30.6 (0.2)	10.2 (0.5)			
6B	σ				29.9 (1.4)	36.7 (0.4)	33.4 (1.5)
7B	σ	59.8 (0.9)	32.7 (0.8)	7.5 (0.3)	30.1 (0.4)	44.0 (0.6)	25.9 (0.6)

μ phase was found to be the stable intermetallic phase over a wide range of alloy compositions.

With increasing Cr level, the third intermetallic which formed was found to be the P phase. Again, it was possible to determine uniquely the three-phase region (γ + μ + P) to define the transition from the μ to the P phase. Alloys #5A and 5B contained both intermetallic phases, μ and P, and the average compositions of the phases in these two samples were used to establish the three-phase field region. In comparison to the μ phase, the P phase existed only over a narrow range of alloy composition as shown in Figure 11.

The final intermetallic phase which was stable at 1123 K was determined to be the sigma phase. Alloy #6B formed both the P and σ precipitates and, therefore, it was possible to determine the three-phase field (γ + P + σ) region.

IV. DISCUSSION

As indicated by the X-ray microanalysis studies, the intermetallic phases in the Ni-Cr-Mo system do not have stoichiometric chemical compositions and the differences in the composition of these phases, particularly for alloys in some of the three phase field regions, were too small to identify them unambiguously by X-ray microanalysis alone. TEM analysis also did not show any reliable morphological differences among the intermetallic phases. Therefore, phases

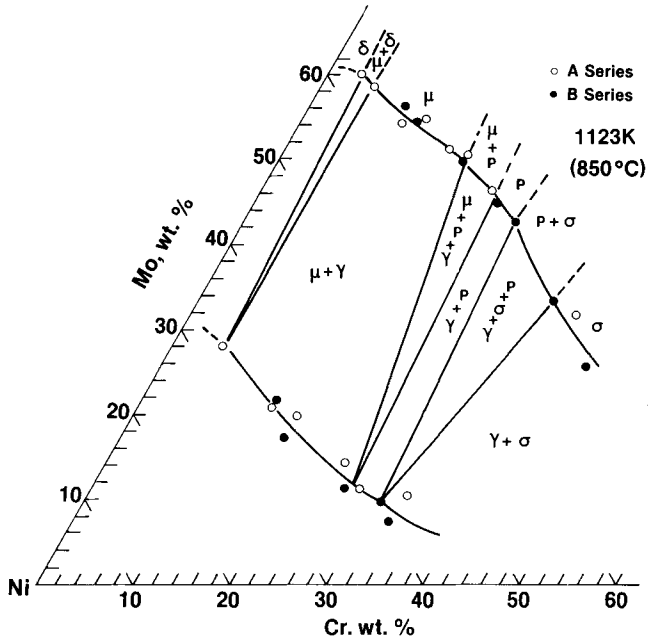

Fig. 11—1123 K (850 °C) section of the Ni-Cr-Mo ternary system as determined in the present investigation.

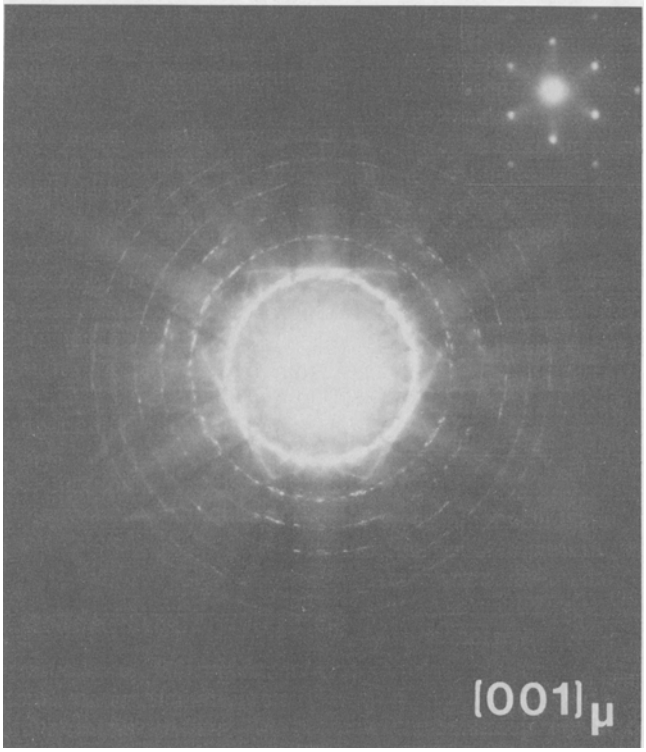

Fig. 12—Convergent beam diffraction (CBD) pattern from $[001]_\mu$ with ZOLZ (inset).

could be identified only by their crystal structure. An examination of the four intermetallic phases found in the system reveals that since their crystal structures and lattice spacing are related, many of their interplanar spacings are comparable. Therefore, the zero layer diffraction patterns from the intermetallic phases in many instances did not provide unique crystal structure identification. Convergent beam diffraction analysis which provides the third dimensional crystal structure and symmetry information was found to be extremely useful to determine unambiguously the crystal structure. This is clearly demonstrated in the CBD pattern of the δ phase shown in Figure 6. The ZOLZ pattern in Figure 6(b) shows a nearly square network of approximately 0.88 nm reflections. This pattern can also be very well indexed as the $[001]_\sigma$ since $d_{100} = d_{010} = 0.88$ nm for the sigma phase. However, the H^{-1} value of 0.9 nm and the two-fold symmetry of the diffraction pattern are not consistent with the $[001]_\sigma$, and for the same reasons the pattern can be correctly indexed as $[010]_\delta$. This indexing can be further supported by demonstrating that the reciprocal lattice points in the first layer should lie directly on the zero layer for this orientation of the δ phase. This uncertainty described above to identify uniquely the crystal structure from the ZOLZ alone is not a unique example but is rather a common problem encountered in complex crystal structures. The indexing of the ZOLZ is further complicated by the fact that the kinematical structure factor extinctions do not always apply and reflections which are forbidden could appear by double diffraction. These diffraction effects have to be taken into account while indexing the ZOLZ. Therefore, the crystal spacing in the third dimension and the symmetry information are extremely useful to distinguish between closely related crystal structures.

The interesting observation in the present study was the formation of the μ phase at 1123 K. As mentioned earlier, μ was found to form in the Fe-W, Co, Mo, and Co-W binary systems. The μ phase is not expected to form in the three binaries of the Ni-Cr-Mo ternary system—*viz.*, Ni-Cr, Cr-Mo, and Mo-Ni—and the present results show that the μ phase is in fact a ternary compound and not an extension from the binary lines. Extensive intermetallic phase formation has been studied in the Ni-Mo binary, but no rhombohedral μ phase formation has been observed.[20,21] This is further supported by analysis in the present study which showed that in the alloys containing the lowest levels of Cr (#1A and #1B), only delta phase was found to form and no μ phase was detected. Thus, the formation of μ phase as a ternary compound is first demonstrated in the present investigation. Similar observations have been made with respect to the sigma phase which forms as a ternary compound (*e.g.*, Fe-Ni-Cr) while the binary systems do not form this phase.[22]

In a recent publication, Barrows and Newkirk proposed a modified PHACOMP approach to predict the formation of intermetallic phases in nickel base alloys[23] and showed good agreement between their predictions and published experimental results. Figure 13 shows the comparison of the 1523 K boundary determined in the present investigation and the calculated boundary based on the approach proposed by Barrows and Newkirk. Ignoring the absence of the triple points in the calculated boundary, the results show good agreement. Similar comparison was also made of the boundaries at 1123 K (Figure 14), and the result shows that there is overall good agreement between the measured and calculated boundaries.

The gamma/gamma + intermetallic phase boundary determined in the present study was compared with the boundaries published by Bloom and Grant[9] and Rideout *et al.*[10] (Figure 15). The boundary reported by Bloom and Grant at

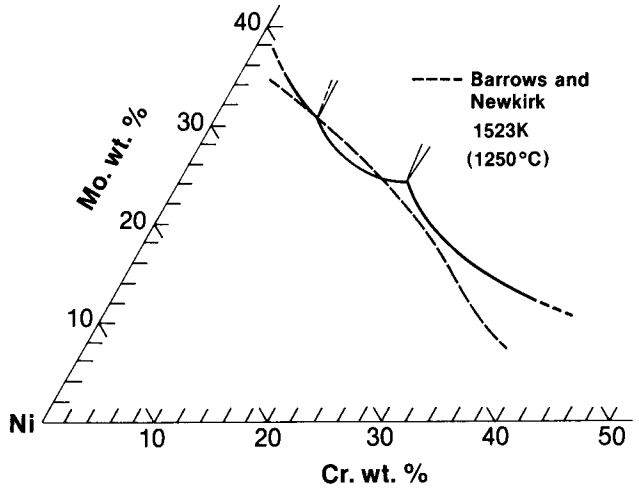

Fig. 13—Comparison of the 1523 K (1250 °C) γ solvus determined in the present investigation with the calculated model proposed by Barrows and Newkirk.[23]

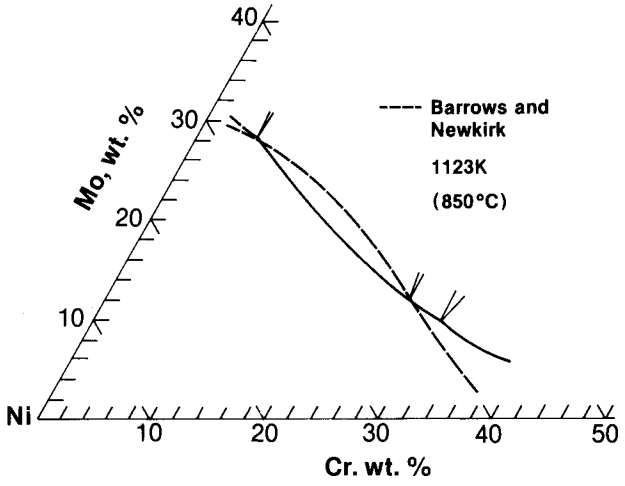

Fig. 14—Comparison of the 1123 K (850 °C) γ solvus determined in the present investigation with the calculated model proposed by Barrows and Newkirk.[23]

1523 K indicates a considerably lower solid solubilities for Cr and Mo in the gamma phase. The boundary reported by Rideout *et al.* at 1473 K shows better agreement with the present results except for some discrepancy in the higher Cr regions. However, the locations of the two gamma triple points ($\gamma/\gamma + P + \delta$ and $\gamma/\gamma + P + \sigma$) were different in all the three studies. Though the exact location of the triple points is difficult to determine using X-ray diffraction, the boundary determined by Rideout *et al.* is reasonably close to the boundary determined in the present study.

The formation of intermetallic phases in Ni-Cr-Mo base alloys such as Hastelloy C 276 has been studied extensively by X-ray diffraction and electron microscopy.[24,25,26] These studies indicated that in addition to the prevalent μ phase, formation of P phase was detected in isolated instances. These observations are consistent with the results of the present investigation which shows that formation of μ and P phases is possible at 1123 K. The alloy additions such as Fe and W in Hastelloy C-276 could easily displace the

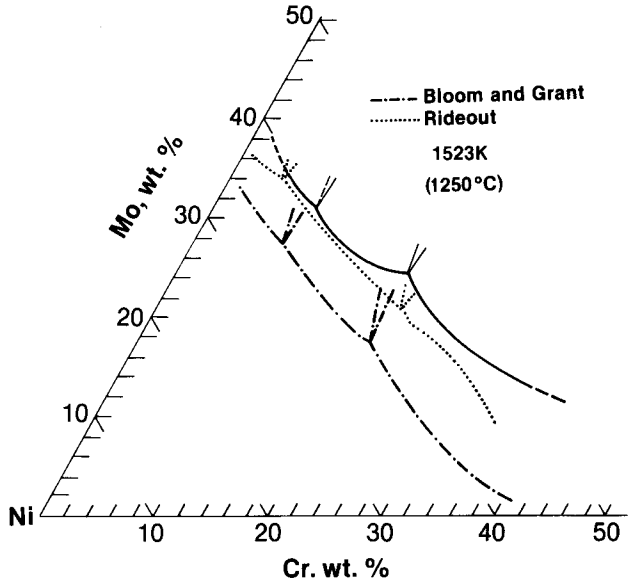

Fig. 15—Comparison of the 1523 K (1250 °C) γ solvus determined in the present investigation with the published results of Bloom and Grant[9] and Rideout *et al.*[10]

gamma solvus line so that the alloy is placed in the three-phase $\gamma + \mu + P$ phase field region.

The determination of phase boundaries using analytical electron microscopy has several advantages. First it should be pointed out that the determination of the phase boundaries by electron microscopy does not require the accurate knowledge of the average bulk composition of the alloy. It has the added advantages of providing tie-line information, the need for fewer samples, and the precise determination of the three-phase field regions. Also, this approach does not assume that the entire sample has a uniform composition and does not preclude the existence of macroscopic inhomogeneities. The procedure only assumes that local equilibrium among the phases is established, and within experimental error would adequately define the phase equilibria. In fact, Romig and Goldstein were able to establish the $\gamma/\gamma + \alpha$ phase boundaries in Fe-meteorites by electron microscopy even when local equilibrium was not reached.[27]

Though the present study provided very encouraging results regarding the ability to determine phase boundaries using an electron microscope, it is necessary to reemphasize the factors which have to be considered to obtain reliable phase boundary information. Most of these factors relate to the accuracy of X-ray microanalysis. First is the contribution of spurious X-rays which can be minimized by procedures outlined.[6] Second, it is necessary to establish accurate k values preferably using single phase standards, the compositions of which are similar to the phases to be analyzed. Third, the size of the second phase particles has to be coarse enough to avoid matrix contributions. If the particle size is small, $\lesssim 0.15$ μm, it is suggested that they be extracted for X-ray microanalysis. Finally, if it is desired that equilibrium be attained among the phases, it may be advantageous to cold deform the samples prior to exposing them to the temperature(s) of interest. The higher defect density will hasten the kinetics to reach equilibrium within reasonable aging times. One of the major shortcomings of

analytical microscopy in the determination of phase boundaries is in systems containing light elements since chemical analysis can be done only by electron energy loss spectroscopy, or by windowless X-ray dispersive analysis. However, these techniques still suffer from both specimen and instrument limitations and quantitative chemical analysis has not been convincingly demonstrated. Further developments in these techniques may permit routine quantitative analysis of light elemental systems in the future.

V. CONCLUSIONS

1. Analytical electron microscopy utilizing X-ray microanalysis and convergent beam electron diffraction analyses was effectively used to determine phase boundaries in the Ni-Cr-Mo system at 1523 K and 1123 K.
2. At 1523 K, intermetallic compounds were determined to be δ, P, and σ phases.
3. At 1123 K, in addition to the above phases, the formation of μ phase was observed. The μ phase formed as a ternary compound.
4. The intermetallic phases could be identified uniquely only by electron diffraction. Due to the similarities in the lattice dimensions of these phases, convergent beam diffraction was extremely useful to unambiguously determine their crystal structures.

REFERENCES

1. R. G. Barrows and J. B. Newkirk: *Metallography*, 1972, vol. 5, p. 515.
2. J. D. Hanawalt, H. W. Rinn, and L. K. Frevel: *Chemical Analysis by X-Ray Diffraction*, Ind. Eng. Chem. Anal. Ed., 1938, vol. 10, p. 457.
3. J. Chipman: *Metall. Trans.*, 1972, vol. 3, p. 55.
4. E. Butchers, G. V. Raynor, and W. Hume-Rothery: *J. Inst. Metals*, 1943, vol. 69, p. 209.
5. J. Bentley, N. J. Zaluzec, E. A. Kenik, and R. W. Carpenter: *Scanning Electron Microscopy*, 1979, vol. 2, p. 581.
6. J. I. Goldstein and D. B. Williams: *Scanning Electron Microscopy*, 1977, vol. 1, p. 651.
7. N. J. Zaluzec: *Introduction to Analytical Electron Microscopy*, J. J. Hren, J. I. Goldstein, and D. C. Joy, eds., Plenum Press, New York, NY, 1979, p. 121.
8. D. B. Williams: "Microanalysis," *Norelco Reporter*, published by Philips Electronic Instruments, Inc., 85 McKee Drive, Mahwah, NJ 07430, 1982, vol. 29, no. 3.
9. D. S. Bloom and N. J. Grant: *Trans. AIME*, 1954, vol. 200, p. 261.
10. S. Rideout, W. D. Manley, E. L. Kamen, B. S. Lement, and P. A. Beck: *Trans. AIME*, 1951, vol. 191, p. 872.
11. G. Cliff and G. W. Lorimer: *Journal of Microscopy*, 1975, vol. 103, p. 203.
12. J. W. Steeds: *Introduction to Analytical Electron Microscopy*, J. J. Hren, J. I. Goldstein, and D. C. Joy, eds., Plenum Press, New York, NY, 1979, p. 387.
13. M. Raghavan, J. Y. Koo, and R. Petkovic-Luton: *J. Metals*, 1983, vol. 35, no. 6.
14. D. B. Williams: "Microdiffraction," *Norelco Reporter*, published by Philips Electronic Instruments, Inc., 85 McKee Drive, Mahwah, NJ 07430, 1983, vol. 30, no. 2.
15. J. I. Goldstein, J. L. Costley, G. W. Lorimer, and S. J. B. Reed: *Scanning Electron Microscopy*, Illinois Institute of Technology Research Institute, 1977, vol. 1, p. 315.
16. C. B. Shoemaker and D. P. Shoemaker: *Acta Cryst.*, 1963, vol. 16, p. 997.
17. J. W. Steeds and N. S. Evans: *Proc. Elec. Micros. Soc. Amer.*, G. W. Bailey, ed., Claitors Publishing Company, Baton Rouge, LA, 1980, p. 188.
18. D. P. Shoemaker, C. B. Shoemaker, and F. C. Wilson: *Acta Cryst.*, 1957, vol. 10, p. 1.
19. E. O. Hall and S. H. Algie: *Metall. Rev.*, 1966, vol. 11, p. 61.
20. *ASM Metals Handbook*, Eighth Ed., American Society for Metals, Metals Park, OH, 1973, vol. 8, p. 426.
21. L. Kaufman and H. Nesor: *Metall. Trans.*, 1974, vol. 5, p. 1617.
22. M. E. Nicholson, C. H. Samans, and F. J. Shortsleeve: *Trans. ASM*, 1951, vol. 44, p. 601.
23. R. G. Barrows and J. B. Newkirk: *Metall. Trans.*, 1972, vol. 3, p. 2889.
24. R. B. Leonard: *Corrosion*, 1969, vol. 25, p. 222.
25. F. G. Hodge and R. W. Kirchner: *Corrosion*, 1976, vol. 32, p. 332.
26. M. Raghavan, B. J. Berkowitz, and J. C. Scanlon: *Metall. Trans. A*, 1982, vol. 13A, p. 979.
27. A. D. Romig and J. I. Goldstein: *Metall. Trans. A*, 1980, vol. 11A, p. 1151.